

A Comparison Study of Two Methods for Elliptic Boundary Value Problems

Jian Du¹, Shuqiang Wang¹, James Glimm^{1,2}, Roman Samulyak²

¹*Department of Applied Mathematics and Statistics,
SUNY at Stony Brook, Stony Brook, NY 11794, USA*

²*Computational Science Center,
Brookhaven National Laboratory, Upton, NY 11973*

April 19, 2018

Abstract

In this paper, we perform a comparison study of two methods (the embedded boundary method and several versions of the mixed finite element method) to solve an elliptic boundary value problem.

1 Introduction

The purpose of this paper is to present a comparative study of two popular methods for the solution of elliptic boundary value problem: the embedded boundary method (EBM) and the mixed finite element methods (MFEM). The methods are quite different in their performance characteristics and the mixed finite element methods could use different basis functions.

To present our main results in an easily accessible manner, we arrange the results in a table of solution time for comparable accuracy. We find that the EBM is better than lower or the same order accurate MFEM, but perhaps not as good as the higher order accurate MFEM we test here.

We observe that no single study of comparison can be definitive, as comparison results may be dependent on the problem chosen, the accuracy desired and comparison method selected. To begin, we distinguish between two not so different kinds of elliptic problems: the elliptic boundary value problems and the elliptic interface problem. For the elliptic boundary value problem, the computational domain exists only on one side of the boundary,

for example, interior/exterior boundary value problem. For the elliptic interface problem, there is some internal boundary called an interface across which the solutions on the two sides satisfy some jump conditions.

There are many methods for solving the elliptic boundary value/interface problems. Several popular methods have been developed on cartesian meshes for the boundary value/interface problems: the immersed boundary method (IBM) by Peskin [12], the immersed interface method by LeVeque and Li [7], the ghost fluid methods (GFM) by Liu, etc. [17], the embedded boundary method by Johansen and Colella [6], integral equation method by Mayo [10], Mckenney, Greengard and Mayo [1]. The advantage of these methods is that they are defined on a cartesian mesh. Therefore no need to generate a mesh. For the cells away from the boundary/interface, they just use a central finite difference method which is simple and second order accurate. For the cells near or crossing the boundary/interface, special treatment is needed. When a (structured/unstructured) mesh is generated before hand, we could use a finite element/finite volume method. It is not easy to get high accuracy by using a finite volume method. The finite element method could have very high accuracy if high order basis functions are used. For elliptic boundary/interface problems, we could use Galerkin finite elements, the discontinuous Galerkin method, and the mixed finite element method. When the boundary/interface is complex, the apparent choice is to use a finite element method (FEM) with an unstructured mesh. However, it is not easy to generate an unstructured mesh especially when the boundary is very complex and the boundary changes with time. Another disadvantage of using FEM with an unstructured mesh is that it does not have the super convergence property which follows when using a uniform structured mesh.

Most of the comparison studies for elliptic boundary value/interface problems are conducted either through mesh refinement or by comparing methods using cartesian mesh [17, 7, 6, 10, 1]. In this paper we are to perform a comparison study of two methods for solving the elliptic boundary value problem: the embedded boundary method using a cartesian mesh and the mixed finite element method using an unstructured mesh. The EBM uses a structured cartesian/rectangle grid. This method uses ghost cells along the boundary and the finite volume method to achieve 2rd accuracy in the potential and flux. The MFEM uses an unstructured triangular mesh. Instead of solving the second order elliptic equation, it solves two first order equations and gives the potential and flux at the same time. Higher order basis functions give higher order of accuracy. Refer to [4] for a thorough discussion of mixed and hybrid finite element methods. For a more implementation oriented view, see [5]. The advantage and disadvantage of the MFEM are briefly discussed in [3]. For the comparison between FEM and

MFEM, see the references cited in [2]. In this paper, we are to use the RT0 (Raviart-Thomas space of degree zero), the RT1 (Raviart-Thomas space of degree one), BDM1 (Brezzi-Douglas-Marini space of degree one) and BDM2 (Brezzi-Douglas-Marini space of degree two) as basis functions of the flux. We use the mixed-hybrid FEM. The final algebraic equations have only the potentials on the mesh edges as unknowns. To use the MFEM, we need to generate the mesh for the computational domain. There are mainly three methods for meshing: the Delaunay triangulation [14], the advancing front method [8] and the quadtree/octree method [9]. In this paper, we use a method based on the quadtree/octree method. This method simplified the original construction by using marching cubes method to recover the interface.

The rest part of the paper is organized as follows. In section 2, we give the discretization of the two methods: embedded boundary method and the mixed finite element method. And also we will show briefly our method of generating the unstructured mesh for the mixed finite element. In section 3, we conduct the comparison study by solving a elliptic boundary problem with a known analytic solution. And in the last section, we give our conclusions.

2 Discretization

We are to solve the elliptic problem:

$$\begin{cases} \phi_{xx} + \phi_{yy} = f \\ \frac{\partial \phi}{\partial n} = g \end{cases} \quad (1)$$

in a complex domain, where $\phi(x, y)$ is called the potential. Since the gradient of the solution $\nabla\phi$ is often needed and more difficult to solve for, we will use the gradient errors as the comparison criterion. The gradients at both the regular grid centers and the boundary points are calculated and compared.

2.1 Embedded Boundary Method

The embedded boundary method is based on the finite volume discretization in grid blocks defined by the rectangular Cartesian grid and the boundary. The solution is treated as a regular block centered quantity, even when these centers are outside of the domain. However the gradient of the potential and the right hand side are located in geometrical centers (centroids) of the partial grid blocks cut by the boundary [6]. This treatment has advantages when dealing with geometrically complex domains; it also ensures second-

order accuracy of the solution.

In the 2D case, each regular grid block is a square. Using the divergence theorem and integrating the flux $\mathbf{F} = \nabla\varphi$ over the control volume, the differential operator can be discretized as

$$(L\varphi)_{\Delta_i} = \frac{1}{V_i}(\sum_j \mathbf{F}_j \cdot \mathbf{S}_j), \quad (2)$$

where V and \mathbf{S} are size of the control volume and block edge respectively, and \mathbf{F} is the flux across the geometric center of each edge. For full edges (not cut by the boundary), \mathbf{F}_j is obtained by the central difference while the flux across the partial block edges is obtained using a linear interpolation between centered difference fluxes in adjacent blocks.

The flux interpolation method is illustrated as the left side of Fig. 1. The flux across the center g of the partial edge ef is obtained using the linear interpolation between the fluxes \mathbf{F}_j and \mathbf{F}_{j+1} , which are the finite differences of potentials at the centers of the corresponding regular grid blocks. The flux at the domain boundary is given by the Neumann condition.

In order to implement the embedded boundary method, the boundary is reconstructed using its intersections with grid lines. The following assumptions and simplifications are made:

1. The maximum number of intersection of each block edge with the boundary curve is one.
2. The elliptic problem domain within each grid block forms a connected set.
3. The positions of the boundary points are adjusted to remove partial blocks with volumes less than a certain preset value.

The first and second assumptions are generally satisfied when the curvature of the boundary curve is not too large or the mesh is sufficiently refined. The third one is necessary since blocks of arbitrary small volumes introduce large numerical errors and increase the condition number of the linear system resulting from the discretization.

The summary of the algorithm is as follows.

(1) The elliptic domain boundary is constructed using intersection points of the grid free boundary with grid lines. All the grid blocks are divided into three types: INTERNAL, PARTIAL, and EXTERNAL, which means completely within, partially within (cut by the boundary), and completely outside of the elliptic domain.

(2) The number of blocks marked as PARTIAL or INTERNAL is counted and the total size of the linear system is set. For each block marked as PARTIAL, all block edges are also divided into three types similar to the types introduced above. The center position and length of each partial edge are stored. A 9-point stencil is set to calculate fluxes across the control volume $BADEF$, as shown in the right side of Figure 1, where the elliptic problem domain is the shaded region and the filled circles represent locations where the potential is defined. We define a 3×3 matrix C with matrix elements $c(i, j)$ representing the coefficient of φ centered at (i, j) ($i, j = 0, 1, 2$) according to $\mathbf{F} = \sum_{i,j} c(i, j)\varphi(i, j)$. Therefore $\varphi(1, 1)$ is always the potential located within the control volume. We further denote $c(i, j)$ as $c(\mathbf{V})$, where the vector \mathbf{V} has components i and j . The vector \mathbf{r} is drawn from the regular block center to the center of the block edge on which the flux is to be integrated. Suppose the basis of the Cartesian coordinate is formed by the unit vectors \mathbf{e}_i ($i = 0, 1$), and \mathbf{e} is the vector with all unit elements, then the unit vector $\mathbf{e}'_i = \text{sign}(\mathbf{r} \cdot \mathbf{e}_i)\mathbf{e}_i$ gives orientational information of \mathbf{r} . For the linearly interpolated flux F along a direction d , the corresponding coefficients are:

$$c(\mathbf{e}) = \frac{a-1}{h_d}; \quad c(\mathbf{e} + \mathbf{e}'_d) = \frac{1-a}{h_d}$$

$$c(\mathbf{e} + \mathbf{e}'_{d'}) = \frac{-a}{h_d}; \quad c(\mathbf{e} + \mathbf{e}'_d + \mathbf{e}'_{d'}) = \frac{a}{h_d}$$

where $d', d = 0, 1$ and $d' \neq d$, h_d is the grid spacing in the direction d , and $a = \frac{|\mathbf{r} \cdot \mathbf{e}_{d'}|}{h_{d'}}$ is the block edge aperture.

(3) Substituting $\mathbf{F} = \sum_{i,j} c(i, j)\varphi(i, j)$ into the equation (2) and summing fluxes through all edges of each PARTIAL block, the coefficients at stencil points are set and added to the global matrix. Note that the right hand side in equation (2) must be evaluated at the centroid of the partial block.

(4) The resulting linear system $A\mathbf{x} = \mathbf{b}$ is solved. Then the gradient of the potential is calculated at all PARTIAL and INTERNAL block centers, even if these centers are outside of the elliptic domain. Either the centered difference or quadric interpolation is used to maintain the second order accuracy. For example, the x-derivative of the potential $\varphi_x(1, 1)$ can be easily calculated by the centered differences of $\varphi(0, 1)$ and $\varphi(2, 1)$. For some points near the boundary, such as point located at $(0, 2)$, $\varphi_x(0, 2)$ is obtained as the x derivative of the quadric curve, which interpolates potential values $\varphi(0, 2)$, $\varphi(1, 2)$, and $\varphi(2, 2)$. We also calculate the gradient of the potential at the boundary points for later comparison. Take the point B in Fig. 1 for example, $\varphi_x(B)$ is the extrapolation between $\varphi_x(H)$ and $\varphi_x(I)$, which in turn are calculated by centered differences. To calculate $\varphi_y(B)$, first we extrapolate

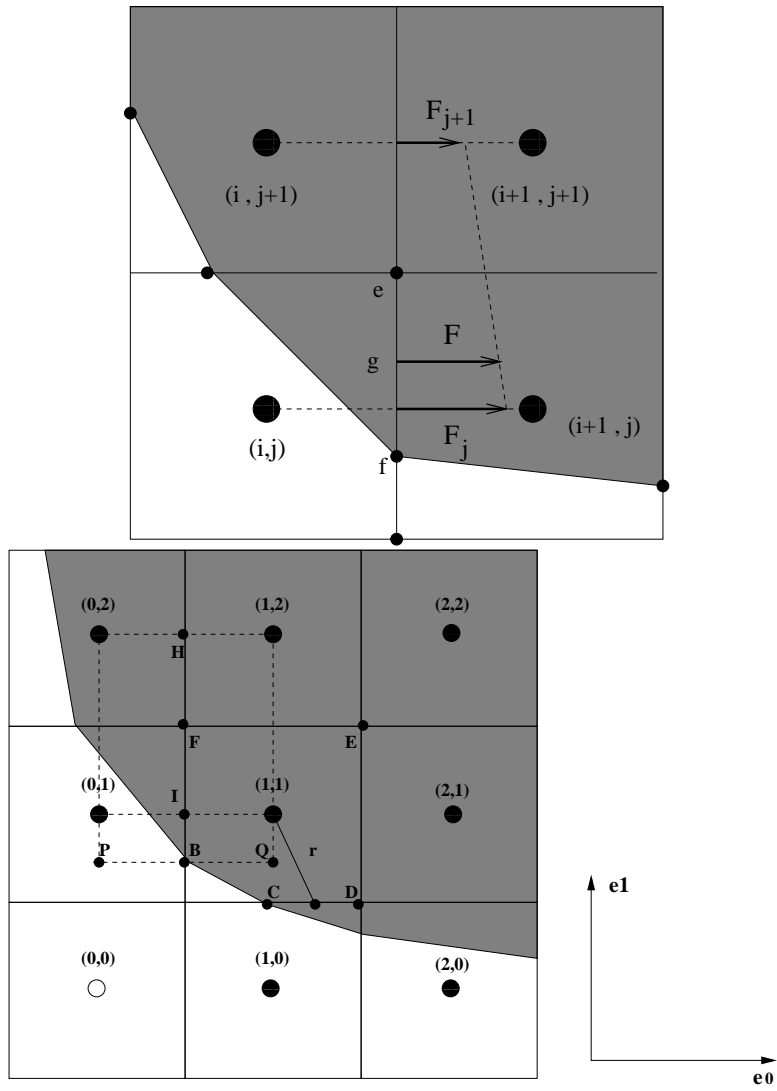


Figure 1: Linear interpolation of flux(Left) and Stencil setting(Right)

$\varphi_y(P)$ from $\varphi_y(0, 1)$ and $\varphi_y(0, 2)$, $\varphi_y(Q)$ from $\varphi_y(1, 1)$ and $\varphi_y(1, 2)$. Then $\varphi_y(B) = \frac{1}{2}(\varphi_y(P) + \varphi_y(Q))$.

2.2 Mixed Finite Element Method

The mixed finite element method (MFEM) solves for the potential ϕ and the flux $\nabla\phi$ at the same time. Thus, it solves

$$\vec{q} = -a\nabla\phi$$

$$\nabla \cdot \vec{q} = f$$

For the mixed finite element method, two function spaces are needed: one scalar space for the potential ϕ and one vector space for the flux \vec{q} . The unknowns are potentials on the elements and flux on the edges. To reduce the problem to a smaller one, the mixed-hybrid finite element is modified by introducing a Lagrangian multiplier on the edges. Chavent and Roberts [5] give in detail an implementation using rectangle elements. The final algebraic equations only have TPs (the Lagrangian multiplier, also the potential on the edges) as unknowns, thus reducing the number of unknowns. Later they reduced the problem further by introducing an unknown variable defined inside the element [2]. Now instead of unknowns defined on edges, they have only one unknown in each triangle element. Since the number of triangles is much smaller than the number of edges, the problem is reduced into a smaller one. However they only use the lowest order RT basis in their derivation. Since we do not know whether their approach could be extended to use higher order basis functions, our implementation uses the first approach [5]. See [4] for a more theoretical treatment of the subject.

In this paper, we use the mixed-hybrid finite element with four different basis functions for the flux: the RT0 (Raviart-Thomas space of degree zero), the RT1 (Raviart-Thomas space of degree one) and BDM1 (Brezzi-Douglas-Marini space of degree one) and BDM2. The basis function for the flux in RT0 is:

$$\vec{s}|_K = a \begin{pmatrix} x \\ y \end{pmatrix} + \begin{pmatrix} b \\ c \end{pmatrix},$$

The basis function for the potential is a constant. The lagrangian multiplier TP defined on edges is also constant. RT0 has 1st order accuracy in the flux and potential in the L_2 norm.

The basis function for the flux in BDM1 is

$$\vec{s}|_K = \begin{pmatrix} a_1x + a_2y + a_3 \\ b_1x + b_2y + b_3 \end{pmatrix},$$

The potential is also constant. However TP is linear. The accuracy for BDM1 is 2nd order in the flux and potential.

The basis function for the flux in RT1 is

$$\vec{s}|_K = \begin{pmatrix} a_1x + a_2y + a_3 & x \\ b_1x + b_2y + b_3 & y \end{pmatrix} \times (c_1x + c_2y),$$

and the basis for the potential is a linear function:

$$v|_K = P_1p_1 + P_2p_2 + P_3p_3,$$

where p_1, p_2, p_3 are the basis functions. TP is also linear. The accuracy is the same as BDM1.

The basis function for the flux in BDM2 is

$$\vec{s}|_K = \begin{pmatrix} a_1x^2 + a_2xy + a_3y^2 + a_4x + a_5y + a_6 \\ b_1x^2 + b_2xy + b_3y^2 + b_4x + b_5y + b_6 \end{pmatrix},$$

The potential is the same as for RT1. TP is quadratic. The accuracy for BDM2 is 3rd order in the flux and potential.

For implementation in details, see [15, 5].

2.3 Mesh Generation

Here, we first introduce our mesh generation method briefly and then give the point location algorithm to locate the triangle which contains a given point. Refer to [15] for more detail.

2.3.1 Quadtree Mesh Generation

For the mixed finite element method, we use an unstructured mesh with triangles only. Our method for mesh generation is similar to the Quadtree/Octree based mesh generation method developed by Yerry and Shephard [9]. However, there is one important simplification in the interface recovering step. The quadtree/octree is a tree structure [13]. Each quadrant in the quadtree has exactly four children and each octant in the octree has exactly eight children. The quadtree/octree is used widely and it is used here for automatic mesh refinement (AMR). The quadtree/octree data structure has a number called level, representing the depth of the tree structure. The root has level 0, its four children has level 1 and so on.

The quadtree/octree mesh generation method is simple and it consists of the following steps (using quadtree as example):

1. Partition the computational region into a quadtree with the level difference between neighbor quadrants being at most 1. Now all those quadrants are either full interior quadrants or partial/boundary quadrants.
2. Triangulate the full interior quadrants.
3. Triangulate the partial quadrants to recover the interface.
4. Post processing the mesh. If we used templates to triangulate the partial quadrants and recover the interface in step 3, we need to move those interface points onto the interface in the post processing step.

The main difference of our method compared with Yerry and Shephard's method [9] lies in the 3rd step in recovering the interface. In their original method, the interface could cross over the edges and on the vertices of the quadtree. In our method, we assume that the interface could only cross over the edges and for each edge, there is at most one crossing. Thus we are using the marching cubes method (MC) for interface recovering. The marching cubes method was proposed by Lorensen and Cline [16] for extracting an isosurface from volumetric data. Here we use it to recover our interface. Note that if the input uses a boundary representation (edges), then our mesh might not be conforming to the input boundary. The reason is apparent when we check the way the constraint delaunay triangulation method recovers the interface: We need to recover the vertices first and then the edges in 2D. For 3D problem, we need to recover the vertices, edges and faces. In our method we recover only edges in 2D and only faces in 3D.

2.3.2 Quadtree Mesh Point Location

After the mesh is given, we use a finite element to set up the matrix and solve for the unknowns. Sometimes we need the solutions for an arbitrary point inside the mesh, which is in fact a point location problem: find the triangle/tetrahedron which contains the given point. The point location problem and another closely related problem called the range search problem are two famous problems in computational geometry. See [11] and references cited therein.

If only one point is queried, we only need to loop through every triangle/tetrahedron of our mesh and test whether the triangle/tetra contains the given point. The time complexity is clearly $O(N)$ where N is the number of triangles/tetrahedra inside the mesh. If m such points are to be queried, such an approach would not be applicable when m is large such as $m = O(N)$. We

would be in such a situation if we solve an elliptic interface problem using the mixed finite element on an unstructured grid and then interpolate the flux back onto an cartesian grid.

To speed up the point location problem, it is a common practice to pre-process the mesh and set up some special data structure. Fortunately, we do not need to create a new data structure here. Since the quadtree/octree is a tree structure, we use it for the point location. Our algorithm is the following:

Given point P, the Quadtree/Octree and mesh,

1. first use the quadtree/octree structure to find a leaf quadrant/octant;
2. second use the leaf quadrant/octant to find an triangle/tetrahedron which would be used as an starting point to find the target triangle/tetrahedron;
3. walk through the mesh to the given point P.

3 A Comparison Study

For our test problem, we use $\phi = e^{\frac{x^2+y^2}{2}}$ as the exact solution of the elliptic equation (1); f and g are obtained by differentiating ϕ . We will show two different testing problems using the same equation and analytic solution. The difference between the two problems lies only in the different boundaries: the second boundary is more complex than the first one. The EBM uses a structured cartesian grid. The mixed finite element methods use an unstructured grid based on the quadtree/octree construction. The quadtree/octree have minimum and maximum levels. In order to compare the results, we need to have comparable grids by letting the minimum/maximum level of the quadtree to be equal. Fig. 2 shows the grid used by the mixed finite element methods when EBM uses the 128×128 grid. Thus the mesh is uniform. We compare the results using the L_2 norm of the flux $\|\nabla\phi\|_2$. The norm is defined as:

$$\begin{cases} \|\nabla\phi\|_2 = \sqrt{\sum_{\text{face}} \|\nabla\phi\|_{2,\text{face}}^2} \\ \|\nabla\phi\|_{2,\text{face}} = \text{Area}(\text{face}) \times \sqrt{\phi_x(x_0, y_0)^2 + \phi_y(x_0, y_0)^2} \end{cases} \quad (3)$$

where (x_0, y_0) is the center of the rectangle for the cartesian grid used by the EBM. For the MFEM, we first interpolate the fluxes at the center of the cartesian grid, and then compute the norm.

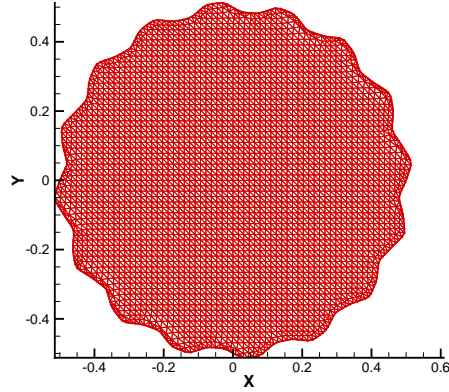


Figure 2: The unstructured computational mesh for a 128×128 mesh

The matrices for both methods are solved using methods in the PETSc package. Here we use the BiCGSTAB method with the ilu method as preconditioner. We have tried different methods (such as lu, Cholesky, CG, GMRES, BiCGSTAB etc) with different preconditioners in the PETSc packages and find that the BiCGSTAD method with ilu as preconditioner is the fastest for solving our matrices.

3.1 Embedded Boundary Method vs. Mixed Finite Element Method

The first problem uses a simple boundary. The computational domain lies inside a perturbed circle as in Fig. 3.

Table 1 displays the errors and timing results for different mesh sizes. The convergence ratios with mesh refinement, the number of unknowns for the linear system, and the number of iterations for the linear solver are also listed. The maximum relative tolerance is $1e^{-9}$. The errors are measured by the L_2 norm of $\nabla\varphi$ defined by (3). From the table, we see that RT0 has only first order accuracy, EBM/BDM1/RT1 have 2nd order accuracy and BDM2 has 3rd order accuracy. The EBM is much faster than the other four methods when the same mesh size is used. The most apparent reason is that it has fewer unknowns than the other four methods. As expected, the RT0 is faster than BDM1/RT1/BDM2 since it has at most one half the number of the unknown variables. However, RT0 only has 1st order accuracy. Although BDM1/RT1 are both 2nd accurate method with the same number of unknowns, they have different characteristics in their timing and accuracy.

Table 1: Convergence and Timing Study using Uniform Mesh for the Boundary in Fig. 3

Mesh Size	EBM				
	error	ratio	time	iterations	unknowns
64×64	1.593569e-04	N/A	0.016966	32	861
128×128	3.670301e-05	2.118	0.099232	60	3338
256×256	8.686625e-06	2.099	0.699156	116	13160
512×512	2.134996e-06	2.074	6.023590	242	52056
Mesh Size	RT0				
	error	ratio	time	iterations	unknowns
64×64	1.011978e-03	N/A	0.193374	74	2642
128×128	5.121661e-04	0.982	0.836596	108	10141
256×256	2.651845e-04	0.950	5.723007	219	39751
512×512	1.353009e-04	0.971	42.336410	462	156715
Mesh Size	BDM1				
	error	ratio	time	iterations	unknowns
64×64	1.329723e-04	N/A	0.475765	87	5286
128×128	3.715907e-05	1.839	3.131988	171	20284
256×256	9.794951e-06	1.924	19.277468	306	79504
512×512	2.538575e-06	1.948	141.012044	597	313432
Mesh Size	RT1				
	error	ratio	time	iterations	unknowns
64×64	1.701312e-05	N/A	0.807441	87	5286
128×128	4.628462e-06	1.878	4.472460	172	20284
256×256	1.215990e-06	1.928	24.581123	305	79504
512×512	3.125208e-07	1.960	163.794142	607	313432
Mesh Size	BDM2				
	error	ratio	time	iterations	unknowns
64×64	4.598191e-07	N/A	1.242945	100	7929
128×128	4.169450e-08	3.463	6.773787	191	30426
256×256	4.824547e-09	3.111	40.007515	317	119256
512×512	2.865473e-09	0.751	336.560434	756	470148

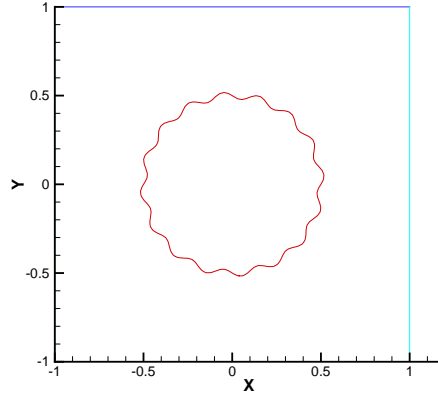


Figure 3: Boundary for the first test

Table 2: timing of RT0 in detail

Mesh Size	RT0		
	mesh	matrix setup/solve	interpolation
64×64	0.083814	0.101778	0.004258
128×128	0.257736	0.547282	0.016645
256×256	0.983702	4.613645	0.073030
512×512	3.849851	37.933463	0.343644

The BDM1 is less accurate but faster for given mesh size. BDM2 has the highest order accuracy of all five methods. For the same order of accuracy, the fastest method is BDM2, then EBM/RT1/BDM1/RT0.

Table 2 gives the timing of the RT0 method for the mesh generation, the matrix setup/solve and the interpolation of the solution. Note that RT0/BDM1/RT1/BDM2 use the same mesh. Therefore their mesh generation time is the same. Their timing differences lie only in the matrix setup/solve step. Here we find that the time spent on generating the mesh is only a small part of the total time when the mesh size is large. Most of the time are spent on solving the algebraic equation (timing for the matrix setup is comparable with that of the interpolation step). It is more apparent when the mesh size is increased. For example, the ratio of time spent on the matrix setup/solve step compared to the mesh generation step is about 1.21 when the 64×64 mesh is used. The same ratio increases to 9.85 when the 512×512 mesh is used.

In the following, we use the EBM and MFEM to solve the same problem but using a more complicated boundary as shown in Fig. 4. The errors are

still measured by the L_2 norm of $\nabla\varphi$ defined by (3) and the max tolerance is $1e^{-9}$. The mesh is more refined in order to well resolve the boundary. Table 3 shows the convergence and timing results of the five methods. The general conclusion is the same as the first test. The RT0 is 1st order accurate, the EBM/BDM1/RT1 method are 2nd order and BDM2 is 3rd order accurate in flux. The EBM method is still the fastest method for the same mesh size. For the same accuracy, we have BDM2, then EBM/RT1/BDM1/RT0 in decreasing order of speed.

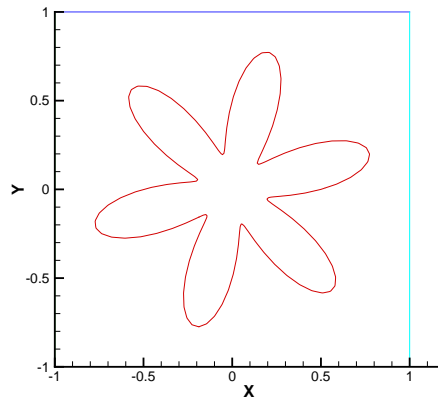


Figure 4: The boundary for the second test

Figs. 5, 6, 7, 8, 9 show the errors for $|\nabla\phi|_2$ using a 128^2 mesh for solving the boundary of Fig. 4.

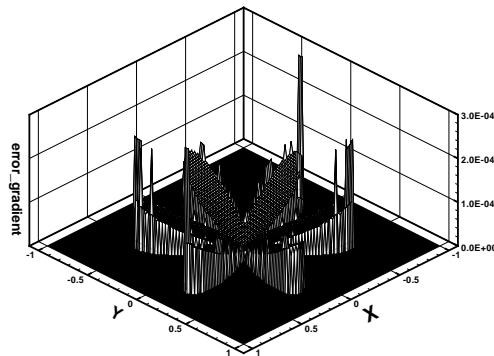


Figure 5: norm of gradient error by EBM using the 128×128 grid

Table 3: Convergence and Timing Study using Uniform Mesh for the Boundary in Fig. 4

Mesh Size	EBM				
	error	ratio	time	iterations	unknowns
64×64	2.110753e-04	N/A	0.022319	43	1008
128×128	5.779287e-05	1.869	0.164115	91	4008
256×256	1.472989e-05	1.920	1.438516	209	15738
512×512	3.641386e-06	1.952	10.398294	360	61967
Mesh Size	RT0				
	error	ratio	time	iterations	unknowns
64×64	1.806532e-03	N/A	0.283352	115	3177
128×128	1.142133e-03	0.661	1.624428	218	12341
256×256	6.140341e-04	0.895	11.236136	415	47870
512×512	3.166839e-04	0.955	79.363582	770	187229
Mesh Size	BDM1				
	error	ratio	time	iterations	unknowns
64×64	1.695040e-04	N/A	0.832989	151	6354
128×128	5.857866e-05	1.533	5.360611	278	24682
256×256	1.641488e-05	1.835	33.627868	461	95740
512×512	4.311759e-06	1.929	320.587307	1185	374458
Mesh Size	RT1				
	error	ratio	time	iterations	unknowns
64×64	2.203143e-05	N/A	1.212332	151	6354
128×128	7.323467e-06	1.589	7.185103	296	24682
256×256	2.032626e-06	1.849	45.390103	549	95740
512×512	5.312876e-07	1.936	312.086512	1055	374458
Mesh Size	BDM2				
	error	ratio	time	iterations	unknowns
64×64	6.651279e-07	N/A	1.916726	176	9531
128×128	7.259815e-08	3.196	12.185872	323	37023
256×256	9.293894e-09	2.966	90.869104	660	143610
512×512	3.087661e-09	1.590	607.406103	1162	561687

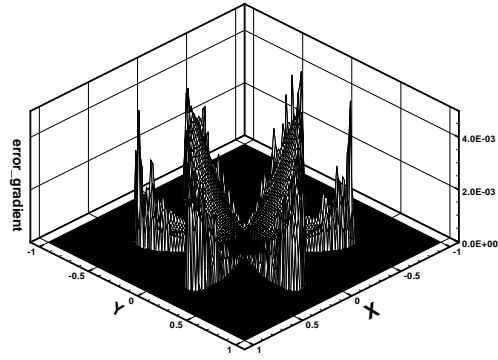


Figure 6: norm of gradient error by RT0 using the 128×128 grid

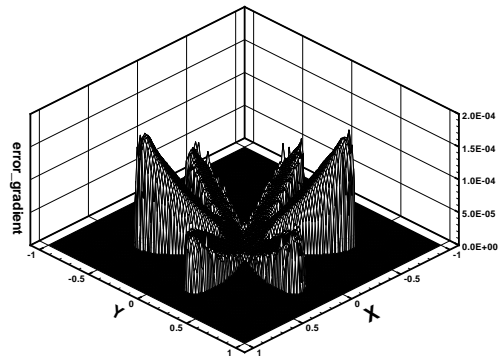


Figure 7: norm of gradient error by BDM1 using the 128×128 grid

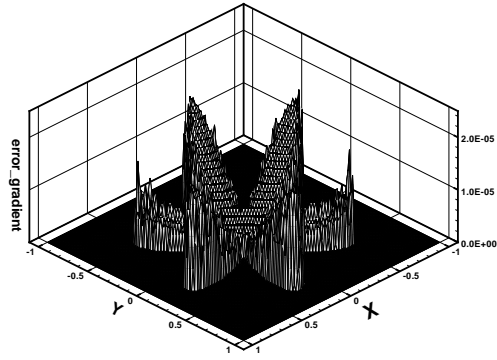


Figure 8: norm of gradient error by RT1 using the 128×128 grid

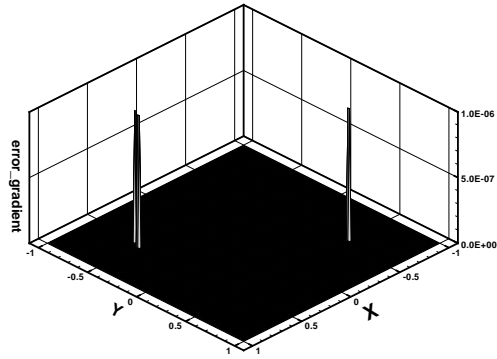


Figure 9: norm of gradient error by BDM2 using the 128×128 grid

Table 4: Maximum gradient errors on the boundary by different methods

Size	EBM	RT0	BDM1	RT1	BDM2
64×64	2.459720e-03	9.367834e-03	7.927028e-04	3.102073e-04	4.988912e-05
128×128	6.567893e-04	6.797467e-03	1.274594e-04	4.007023e-05	1.038527e-06
256×256	1.755489e-04	3.626596e-03	2.486447e-05	1.321007e-05	1.033665e-07
512×512	4.614643e-05	1.754357e-03	6.351849e-06	2.751578e-06	2.310828e-08

In Table 4, we show the maximum gradient errors on the boundary by different methods. From this table, we know that the order of accuracies of maximum gradient errors on the boundary for the five methods are comparable with the L_2 norm on the whole domain.

3.2 Automatic Mesh Refinement vs. Uniform Grid

In this section, we compare the convergence rates when the mesh is refined around the boundary. The boundary is the same as the boundary of Fig. 4 for our second test. We only compute the results using RT1. Figure 10 shows the mesh when the quadtree's minimum level is 6 and maximum level is 9. And Fig. 11 gives the flux error plot. From Table 5 we see that the refinement does not give a more accurate solution on the whole computational domain. In fact, this is reasonable. From Fig. 11, we know that the maximum errors are located in the interior where the mesh is coarsest, where the mesh is not refined. Our refinement is only around the boundary and in this way the errors near the boundary are reduced. The effect of boundary flux error reduction by mesh refinement diminish gradually.

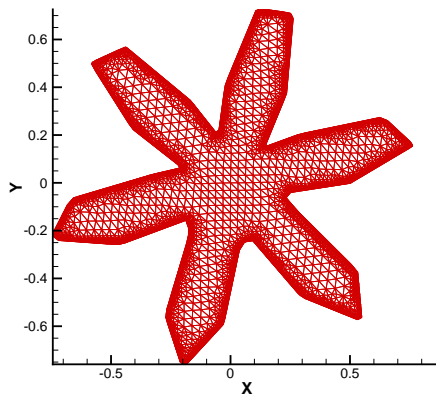


Figure 10: Mesh when minimum level is 6 and maximum level is 9

Table 5: Convergence and timing results for automatic mesh refinement (minimum level = 6) using RT1 for the domain of Fig. 4

maximum level	RT1				unknown number
	error	max boundary error	time	iterations	
6	2.203159e-05	3.102045e-04	1.461276	151	6354
7	1.766854e-05	4.128689e-05	2.533742	224	11200
8	1.539364e-05	8.678919e-06	7.155402	330	22758
9	1.462538e-05	3.401366e-06	20.458581	467	47214
10	1.387916e-05	8.151048e-07	68.288392	789	96076

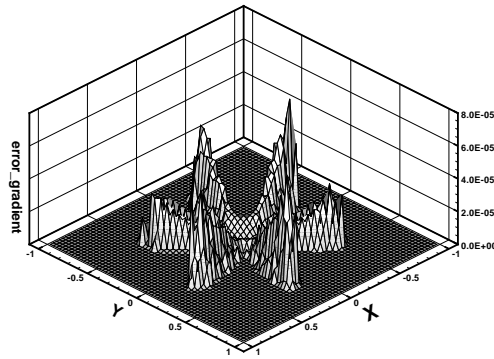


Figure 11: Flux error when minimum level is 6 and maximum level is 9

4 Conclusion

In this paper, we have used the embedded boundary method and the mixed finite element method to solve the elliptic boundary value problem in 2D. We compared the convergence and timing results.

Since the embedded boundary method uses a structured cartesian grid, it is easier to implement. It is much harder to write the mesh generation program. But after the mesh is given, the discretization is simpler for the mixed finite element method. And it is easier to use the mixed finite element for the elliptic interface problem since the interface is in fact an internal boundary. However, the EBM method must be modified to solve an elliptic interface problem. To save computational resources when solving large problems, we could use EBM with automatic mesh refinement, which is one important part

of our mesh generation method.

The EBM has the advantage of fewer unknowns with the same mesh size compared with the MFM. There are two reasons for this. One reason is that the EBM uses a structured grid and the finite volume/central finite difference has super convergence in the mesh. The MFM uses an unstructured grid, and to achieve the same order of accuracy, a higher order basis function space is needed, which means more unknowns. The other reason is that the unknowns for EBM are cell centered and those for the MFM are edge centered. Since the approximate ratio of the vertices to faces to edges is 1:2:3 for a simple large triangle mesh, we know the ratio of the unknowns for the EBM, RT0, BDM1, RT1, BDM2 is approximately 1:3:6:6:9. Thus the EBM problem is smaller, which explains why it is much more faster. However, for a given accuracy, the fastest method is BDM2 which is 3rd order accurate in flux, and then EBM/RT1/BDM1/RT0.

References

- [1] A. Mayo A. Mckenney, L. Greengard. A fast poisson solver for complex geometries. *J. Comput. Phys.*, 118:348C355, 1995.
- [2] P. Ackerer A. Younes, R. Mose and G. Chavent. A new formulation of the mixed finite element method for solving elliptic and parabolic pde with triangular elements. *J. Comput. Phys.*, 149(1):148–167, 1999.
- [3] Douglas N. Arnold. Mixed finite element methods for elliptic problems. *Comput. Methods Appl. Mech. Engrg.*, 82:281–300, 1990.
- [4] Franco Brezzi and Michel Fortin. *Mixed and Hybrid Finite Element Methods*. Springer Series In Computational Mathematics 15, 1991.
- [5] G. Chavent and J.E. Roberts. A unified physical presentation of mixed, mixed-hybrid finite elements and standard finite difference approximations for the determination of velocities in waterflow problems. *Adv. Water Resources*, 14(6):329–348, 1991.
- [6] P. Colella H. Johansen. A cartesian grid embedding boundary method for poisson’s equation on irregular domains. *J. Comput. Phys.*, 147:60C85, 1998.
- [7] R.J. LeVeque and Z.L. Li. The immersed interface method for elliptic equations with discontinuous coefficients and singular sources. *SIAM J. Numer. Anal.*, 31:1019C1044, 1994.

- [8] D. L. Marcum. Efficient generation of high-quality unstructured surface and volume grids. *Engineering with Computers*, 17(3):211–233, 2001.
- [9] M.S.Shephard M.A.Yerry. A modified quadtree approach to finite element generation. *IEEE Comput. Graph. Appl.*, 3(1):39–46, 1983.
- [10] A. Mayo. The fast solution of poisson’s and the biharmonic equations on irregular regions. *SIAM J. Numer. Anal.*, 21:285C299, 1984.
- [11] M. Overmars M.D. Berg, M.V. Kreveld and O. Schwarzkopf. *Computational Geometry: Algorithms and Applications*. Springer, second edition edition, 1998.
- [12] Charles S. Perskin. The immersed boundary method. *Acta Numerica*, 11:479–517, 2002.
- [13] Hanan Samet. *The design and analysis of spatial data structures*. Addison-Wesley Series In Computer Science, 1990.
- [14] Jonathan Richard Shewchuk. *Delaunay Refinement Mesh Generation*. PhD thesis, Computer Science Department, Carnegie Mellon University, May 1997.
- [15] Shuqiang Wang. *A Mixed Finite Element Method for Elliptic Interface/Boundary Value Problem*. PhD thesis, SUNY at Stony Brook, August 2006.
- [16] H.E. Cline W.E. Lorensen. Marching cubes: a high resolution 3d surface construction algorithm. *Computer Graphics*, 21(4):163–169, 1987.
- [17] M. Kang X.D. Liu, R.P. Fedkiw. A boundary condition capturing method for poisson’s equation on irregular domains. *J. Comput. Phys.*, 160, 2000.